# Thermal, Mechanical, and Adhesive Properties of HDPE/ Reactive Ethylene Terpolymer Blends

**C. T. Love,[1] G. Xian,[2] V. M. Karbhari[1,2]**

[1]*Materials Science and Engineering Program, University of California, San Diego, La Jolla, California*
[2]*Department of Structural Engineering, University of California, San Diego, La Jolla, California*

Received 11 November 2005; accepted 26 December 2005
DOI 10.1002/app.24050
Published online in Wiley InterScience (www.interscience.wiley.com).

**ABSTRACT:** Blends of high-density polyethylene (HDPE) and a reactive ethylene terpolymer (RET) were developed as a protective coating material for steel. A morphological study with scanning electron microscopy (SEM) indicated that blends of HDPE and RET are immiscible, while high interaction between these two phases was found. Crystallization and thermomechanical behavior of the blends were investigated using differential scanning calorimetry (DSC) and dynamic mechanical thermal analysis (DMTA). The crystallinity of HDPE decreased with the incorporation of RET slightly due to the disturbance of the highly viscous RET melt during crystallization. Tensile tests indicated that the addition of RET reduced both strength and modulus but increased the strain-to-break. Adhesion to steel substrates was improved with the incorporation of the RET component. An optimum composition of RET loading was detected to be in the range of 25–33 wt %, leading to the best adhesive performance, high tensile strength, and strain-to-failure of the blend material. © 2007 Wiley Periodicals, Inc. J Appl Polym Sci 104: 331–338, 2007

**Key words:** adhesion; blend; polyethylene; compatibility; crystallization

## INTRODUCTION

The development of protective coatings for corrosion control of metals is continually important in the marine, oil and gas industries. Sufficient coatings for steel structures must be tough, abrasion resistant, impermeable to attack from moisture and chemicals, easily applied in-the-field, resistant to cathodic reactions, and of course highly adhesive to the substrate to be protected.[1] The use of thermoplastic polymer materials is gaining increasing acceptance over thermosetting materials for such applications due to the ability for quick in-the-field bonding using a variety of bonding methods.[2,3] Hot-melt thermoplastics eliminate the need for environmentally harmful solvents which reduce curing time and reduce emissions, making them a more environmentally friendly alternative.[4,5] Additionally, thermoplastic coatings may be applied in various thicknesses, whereas thermoset epoxies must be applied in thin, often brittle layers. Perhaps the most commonly used thermoplastic in such applications is polyethylene due to its resistance to chemical and moisture attack and high toughness.[6] However, the implementation of polyethylene by itself is limited by poor adhesive properties because of its inherent nonpolar nature. Blending high-density polyethylene (HDPE) with polar copolymers has been shown to help increase adhesion between polymer coatings and high surface energy steel substrates.[7–10]

Historically, high adhesive strength and compatibility have been best established by coatings containing ethylene copolymer ionomers, containing sodium-, zinc-, or lithium-ion neutralized ethylene methacrylic acid copolymers.[11–17] These materials possess the desired toughness, impact resistance, and adhesion but are sensitive to the permeability of moisture. Reactive olefin copolymers provide an alternative where lack of permeability is of great importance for the durability and reliability of the coatings, as in the case of offshore structures and naval vessels. Glycidyl methacrylate (GMA) containing ethylene copolymers (ethylene/methyl acrylate/glycidyl methacrylate) have been successfully applied to compatibilize poly(ethylene terephthalate) (PET) and HDPE.[18] As indicated, the epoxy functionality of GMA provides a high reactivity in relation to the end group of PET, while the ethylene sequence is expected to ensure adhesion to the HDPE.[18] The content of GMA within the copolymer decides the miscibility and thus the mechanical and thermal properties of the blend of HDPE and the copolymer.[18] The increase of GMA content of the copolymer deteriorates the miscibility between the copolymer with HDPE. In the present study, a reactive ethylene terpolymer (RET) of ethylene/*n*-butyl acry-

*Correspondence to:* V. M. Karbhari (vkarbhari@ucsd.edu).
Contract grant sponsor: E.I. DuPont de Nemours and Company.

late/glycidyl methacrylate (E/nBA/GMA) was applied to blend with HDPE to develop a potential coating material. As expected, the HDPE component offers high chemical and moisture resistance,[8] while the RET component provides the material with high polarity and reactivity, which will enhance adhesion to the substrates to be coated. Unpublished results by the author show low-density polyethylene/RET systems to have inferior mechanical properties necessary for advanced polymeric coatings. Out of convenience, the blends of RET and HDPE in all compositions were prepared by reciprocating screw injection molding rather than a twin screw extruder compounding routine. This one step melt processing proved satisfactory for mixing HDPE with PET with and without a compatibilizer.[18] Additionally, it is of great importance from an industrial point of view due to high efficiency. The injection molded blends were investigated on their morphology, thermal, and mechanical properties as well as the adhesive strength to the metal substrates. The study is believed to help completely assess the application of the blend materials as a coating material.

## EXPERIMENTAL

### Materials

Pure HDPE with melt flow index (MFI) of 1 g/10 min and molecular weight ($M_w$) of 125,000 was purchased from Scientific Polymer Products™. The GMA-containing terpolymer, RET (Elvaloy 4170®), was offered by the DuPont™ company. The terpolymer contains an ethylene backbone with *n*-butyl acrylate, an elastomeric toughening agent and glycidyl methacrylate, a dual functionality epoxidized adhesion promoter. The density and the MFI of the RET are 0.94 g/cm$^3$ and 12 g/10 min, respectively.

A silane coupling agent, γ-aminopropyltriethoxysilane (Aldrich™) was applied to treat the surfaces of steel coupons for lap shear tests. The steel coupons (101.6 × 25.4 × 1.53 mm$^3$) were cut from structural grade, A36, hot-rolled steel plates.

### Preparation of polymer blend

A reciprocating screw injection molder was used to facilitate mixing of the RET and HDPE, and to produce "dog-bone" tensile samples. The dimensions of the injection molded sample are 165 mm overall length, 50 mm gauge length, and 3.2 mm thickness, as specified for Type I testing in ASTM D 368. Three injection molder heat zones were kept constant at 190°C with the mold heat at 40°C to minimize coupon shrinkage. Prior to injection molding, the RET was dried at 60°C overnight to remove absorbed moisture. The prepared blends include 25, 33, 50, 66, and 75 wt % RET, and are designated HDPE 75/25, HDPE 66/33, HDPE 50/50, HDPE 33/66, and HDPE 25/75 in the following text, respectively.

### Material characterization

#### Scanning electron microscopy

A scanning electron microscope was used to investigate the morphology of the blends. Cryofractured surfaces were examined with and without etch. Etched specimens were placed in toluene for 90 min to preferentially remove the RET component. Samples were pressed against carbon tape mounted on aluminum stubs. A thin layer (~40 Å) of gold/palladium alloy was sputter coated on the fractured surfaces.

#### Differential scanning calorimetry

A differential scanning calorimeter was used to determine the degree of crystallinity ($X_c$) and melting temperature ($T_m$) of pure HDPE, RET, and their blends. Samples of ~15 mg were taken from injection molded coupons. For HDPE and its blends, the heat profile went as follows: sample were scanned up to 150°C from 10°C at a heating rate of 10°C/min, annealed at 150°C for 3 min, and then cooled down to 10°C at a rate of about 2°C/min with $N_2$ purge gas at a flow rate of 10 mL/min. For the pure RET, the maximum heating temperature was set to 100°C, to ensure complete melting while avoiding degradation for further scans. All other conditions were similar to that for polyethylene. Scans were re-run with the subsequent scan reported to eliminate the thermal history effects of the injection molding process. Observing the melt behavior in the second scan better represents the morphology of the two component blend. Crystallinity was determined using the ratio of the melting enthalpy of samples to that of a perfect and infinite polyethylene crystal, $\Delta H_{m,\mathrm{HDPE}}{}^0 = 292$ J/g.[19] The degree of crystallinity ($X_c$) for HDPE was estimated using eq. (1):

$$X_c = \frac{\Delta H_m}{\Delta H^0_{m,\mathrm{HDPE}}} \quad (1)$$

where $\Delta H_m$ is the melting enthalpy.

#### Dynamic mechanical thermal analysis

A dynamic mechanical thermal analyzer with a three-point bending fixture was used to determine the viscoelastic properties. Specimens (35 × 10 × 4 mm$^3$) cut from the injection molded coupons were tested from −140°C to 140°C (110°C for pure RET sample) at 2°C/min with 1 Hz frequency and 0.025 strain. Liquid nitrogen was used for achieving subambient temperature.

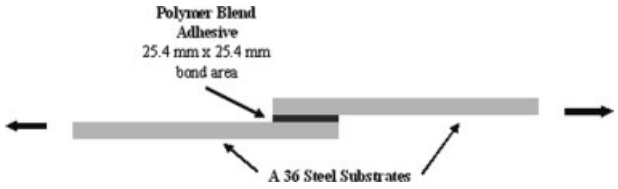


**Figure 1** Lap-shear adhesion testing schematic.

### Tensile testing

Tensile testing was performed according to ASTM D638. Sand paper was used in the machine grips to avoid pull-out and "slippage." The extension rate was 50 mm/min and all tests were performed at room temperature. Five samples were tested for each blend composition with representative properties reported.

### Single-lap adhesive test

Lap shear adhesion testing consisted of the polymer blend hot-melt bonded between structural grade (A36) hot-rolled steel coupons of dimensions 25.4 $\times$ 101.6 mm$^2$ and thickness 1.53 mm. Two surface pretreatment techniques were performed on steel substrates. Polished surfaces were achieved using 320-grit silicon carbide paper and a rotary polishing wheel. Sand-blasted surfaces were achieved using 320-grit roughening media. A silane coupling agent, $\gamma$-aminopropyltriethoxysilane (Aldrich), was employed in several adhesive measurements. Two concentrations of silane (3 and 10 vol %) in a methanol/ethanol solution were produced to achieve varying silane layer thicknesses on steel. While more sophisticated surface pretreatment techniques such as laser roughening and corona discharge could be employed to maximize adhesive performance, they were not considered in this work as they prove to be impractical for in-the-field applications.

Metal/polymer/metal lap-shear joints were prepared using the polymer blend as an adhesive. Steel coupons were acid etched to remove an anticorrosion chemical treatment from the manufacturer and wiped clean with acetone prior to bonding. The thin polymer films, thickness of $\sim$0.4 mm, were cut to an area of 645 mm$^2$ (1 square inch) which represented the total bonding area. Metal/polymer/metal joints were preheated to 215°C without pressure for 3 min. A pressure of 3.8 MPa was then applied for 3 min before removing the joint from the press and cooling to room temperature. A diagram of the produced lap-shear joint for testing is given in Figure 1. The adhesive performance of the lap-shear joints was evaluated using a servo-hydraulic Instron tension testing machine. Sample joints were loaded to failure according to ASTM D 5868 at 13 mm/min for similar adhesive joints. Equation (2) was used to find the adhesive strength, $\sigma_{\mathrm{Adh}}$, of the polymer blends bonded to steel.

$$\sigma_{\mathrm{Adh}} = \frac{P_{\mathrm{Max}}}{A_{\mathrm{Bond}}} \tag{2}$$

where $P_{\mathrm{Max}}$ is the maximum load at or before rupture and $A_{\mathrm{Bond}}$ is the area of overlap bonding (645 mm$^2$). Fracture surfaces were observed to qualitatively characterize failure as being associated with adhesion, cohesion, or mixed adhesion/cohesion. For purposes of this investigation, cohesion is defined as polymer product left bonded to both lap-shear substrates. Adhesion is defined by a clean substrate surface free of residual adhesive polymer.

## RESULTS AND DISCUSSION

### Morphology, thermal, and mechanical properties of blends

The scanning electron micrographs of cryofractured polymer surfaces illustrated in Figure 2 show the two phase morphology, indicating immiscibility of the

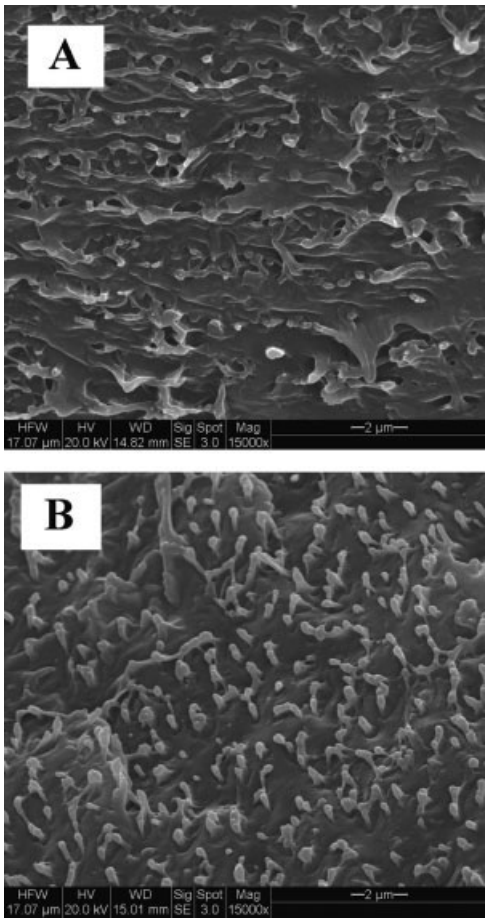


**Figure 2** Scanning electron micrographs of cryofractured HDPE/RET blends: (A) HDPE 66/33 and (B) HDPE 33/66.

blends at 33 and 66 wt % RET. It has been suggested that such immiscibility may result from the difference in chain polarity as in the case of HDPE/ionomer polymer blends.[20] This behavior is also well documented in other instances of olefin/olefin-containing blends.[20–24] The terpolymer appears as short rod-shaped segments dispersed in an HDPE matrix with greater inclusion density found at higher RET content. During freeze fracture, RET segments were strained, causing "pull-out" and the formation of voids surrounding the inclusions. The rod diameter is approximately 0.3–0.5 $\mu$m. The improvements of elongation-at-break and adhesive strength of HDPE when blended with RET come from the compatibility similar to that shown in HDPE/PET systems.[18]

The SEM micrographs in Figure 3 illustrate the morphological effect of adding RET to the blend, where the RET has been removed via etching. In blend HDPE 75/25 [Fig. 3(A)], the RET appears as small spherical and elongated inclusions dispersed evenly throughout the continuous HDPE matrix. A range of spherical diameters and ellipsoidal lengths approximately fall within 0.3–0.6 $\mu$m for diameter and 0.3–1.3 $\mu$m for the ellipsoidal length. As RET content increases to 33% [Fig. 3(B)] the RET inclusions coalesce and further elongate in the injection molding direction into irregular domains within the HDPE matrix. The ellipsoidal length of RET inclusions at this composition were shown to extend past 14 $\mu$m. The tendency towards coalescence of elastomeric particles added to brittle matrices and the elongation thereof has been shown in polyethylene/ethylene vinyl acetate (PE/EVA) blends at 30 wt % EVA[25] and in an HDPE/solid silicone system.[26] Likewise, a decrease in matrix domain size is seen with increasing compatibilizer content in poly(butylene terephthalate)/polypropylene system where the compatibilizer is similar to the glycidyl methacrylate component present in the RET system used here.[27] The morphology in Figure 3(C) (HDPE 33/66) is more consistent with a two phase cocontinuous matrix in which both HDPE and RET coexist. Interestingly, the rod-shaped RET inclusions shown in Figure 2(B) are also seen within HDPE domains in Figure 3(C) (indicated by arrows). This is possible because the etch technique used was done purely to remove RET at the cryofractured surface. In both conditions of etched and nonetched, the inclusion approximate inclusion diameter remains the same (0.3–0.6 $\mu$m).

The melting thermograms of HDPE, RET, and their blends are shown in Figure 4. No distinct melting peak is seen for pure RET but rather a broad distribution of melting temperatures ranging from 29.9°C to 87°C; which becomes less distinct as RET content decreases. A repeat test supported this observation, identifying the existence of a melting zone, rather than a distinct melting point for the RET. This zone includes the manufacturer reported melting temperature of $T_{m,\mathrm{RET}} = 72$°C. It has been presented elsewhere that melting temperature for a semicrystalline polymer is related to the lamellar thickness.[28] The melting zone measured in the present study may indicate a broad distribution of the crystalline lamellar thickness in the RET. Considering the complex molecular structure of the copolymers in the RET, it is reasonable to assume that the arrangement of the —$CH_2$—$CH_2$— molecular seg-

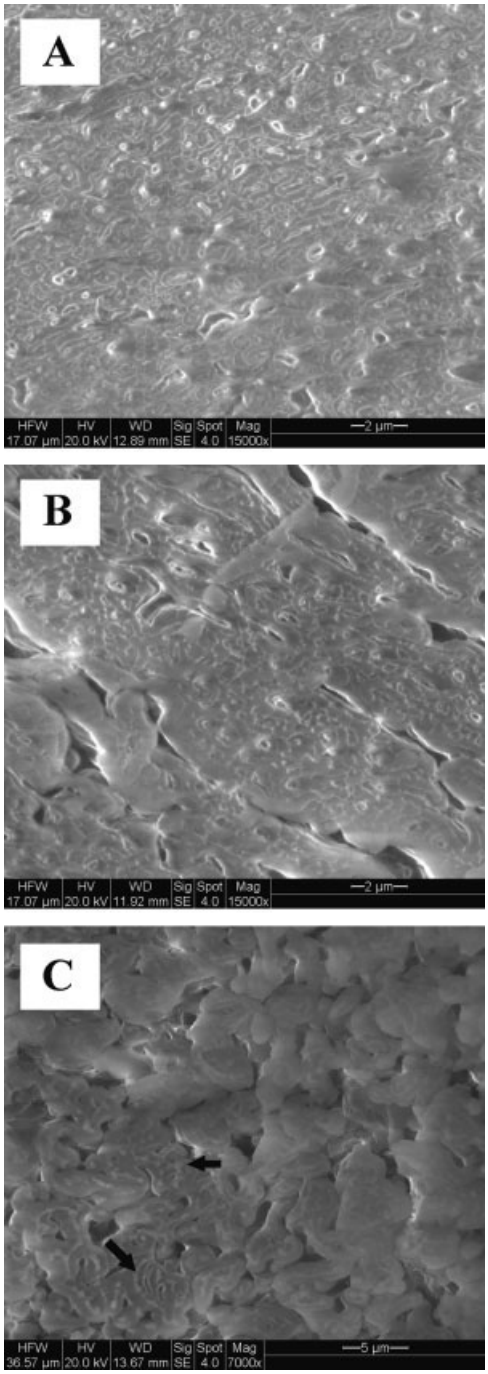


**Figure 3** Scanning electron micrographs of etched cryofractured HDPE/RET blends; (A) HDPE 75/25; (B) HDPE 66/33; (C) HDPE 33/66.

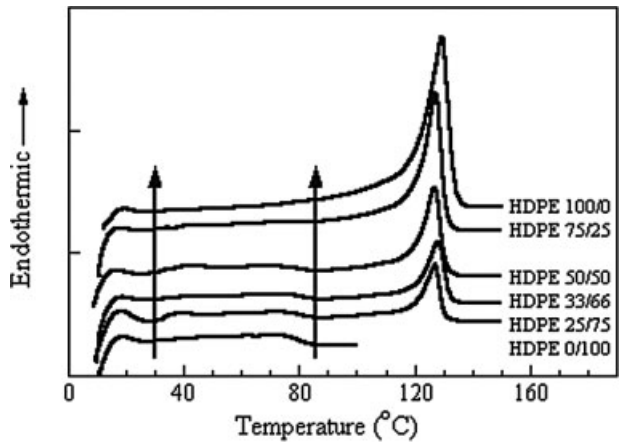


**Figure 4** DSC melting thermograms of HDPE, RET, and their blends.

ment into a regular crystalline structure is blocked or limited by the butyl-acrylate and glycidyl methacrylate segments. This may lead to a range of crystalline lamellar thickness and melting temperatures. As for HDPE, the melting temperature was found to be 129.6°C, in accordance with previous reports.[28] The incorporation of RET decreases the melting temperature of HDPE slightly as shown in Table I. The distinct melting zone for RET and peak for HDPE of the blends indicate that separate crystals formed during crystallization of the blends, which illustrate immiscibility in the crystalline phases.[20] This is expected due to the immiscibility of HDPE and the RET (Fig. 3).

The effect of RET content on $T_m$ of HDPE and its blends is shown in Table I. The addition of RET reduces $T_{m,\mathrm{HDPE}}$ only slightly, while the magnitude of the endotherm peak (Fig. 4) decreases significantly with increasing RET content. Likewise, the melting zone for the RET remains uniform but increases in magnitude with increasing RET content. The small decrease of $T_m$ of HDPE may be explained by a decrease in HDPE crystalline lamellar thickness, to a small extent, because of the disturbance of RET molecules during crystallization.

The variation of the blend crystallinity with RET content is presented in Table I. For HDPE, the addition of the RET suppresses crystallinity. Note that the crystallizing temperature for HDPE is around 110°C,[28] at which temperature RET is in the complete melting state. In this case, it is a reasonable assumption that the crystallinity of HDPE is affected by the RET melt. The decrease in crystallinity of the blend suggests that RET shows a negative effect on the crystallizing process of HDPE. This may be due to the high viscosity of the RET melt or the extent of entanglement between nBA and GMA copolymers, which constrains the motion of HDPE molecular chain during crystallization.

A plot of the tan δ loss factor versus temperature for HDPE/RET blends is shown in Figure 5. Peaks below the melting point of HDPE are designated as α, β, and γ relaxations. The γ transition serves as the primary $T_g$ for pure HDPE (HDPE 100/0) at −120°C. This $T_g$ value is one among many cited in the literature.[8,29] As for the RET, there is no γ transition seen in this reported temperature range. The addition of RET leads the position of the γ transition to shift to lower temperature, indicating the enhanced motion of molecular segments in the amorphous phase.

The peak in the tan δ curve over the β transition serves as the $T_g$ for pure RET at −40°C. This transition increased from −40°C (HDPE 0/100) to −33°C (HDPE 75/25), suggesting that HDPE shows a constraining effect on the molecular segment motion. This is related to good interfacial interaction and adhesion between the two phases.

The α transition for pure HDPE shows a broad peak around 51°C. This may result from the high degree of crystallinity ($X_c$ = 43%), where sharp tan δ peaks are often only observed in amorphous polymers.[8] The storage modulus ($E'$) versus temperature for HDPE/RET blends in Table I illustrates that as RET content increases, storage modulus decreases.

Representative tensile testing stress–strain curves show the physical effects of blending RET with pure HDPE. Typical stress–extension curves are shown in Figure 6. The large plastic deformation and ductile

**TABLE I**
**Thermal Characteristics of HDPE/RET Blends**

| HDPE/RET (wt %) | Melting temperature (°C) | | Storage modulus, $E'$ (GPa) | | | | Crystallinity (%) |
|---|---|---|---|---|---|---|---|
| | $T_{m,\mathrm{RET}}$ | $T_{m,\mathrm{HDPE}}$ | −100°C | −50°C | 0°C | 50°C | $X_{c,\mathrm{HDPE}}$ |
| 100/0 | – | 129.8 | 3.0 | 2.5 | 1.8 | 0.9 | 42.9 |
| 75/25 | 31.9–82.5 | 128.0 | 1.8 | 1.3 | 0.6 | 0.2 | 40.6 |
| 66/33 | 30.9–86.1 | 129.0 | 1.9 | 1.7 | 0.7 | 0.2 | 41.4 |
| 50/50 | 29.9–85.3 | 128.4 | 1.7 | 1.3 | 0.2 | 0.1 | 35.8 |
| 33/66 | 31.0–84.5 | 128.5 | 1.0 | 1.1 | 0.2 | 0.1 | 36.9 |
| 25/75 | 31.6–85.1 | 127.2 | 1.9 | 1.1 | 0.2 | 0.1 | 39.5 |
| 0/100 | 29.5–87.0 | – | 1.1 | 0.5 | 0.03 | 0.005 | – |

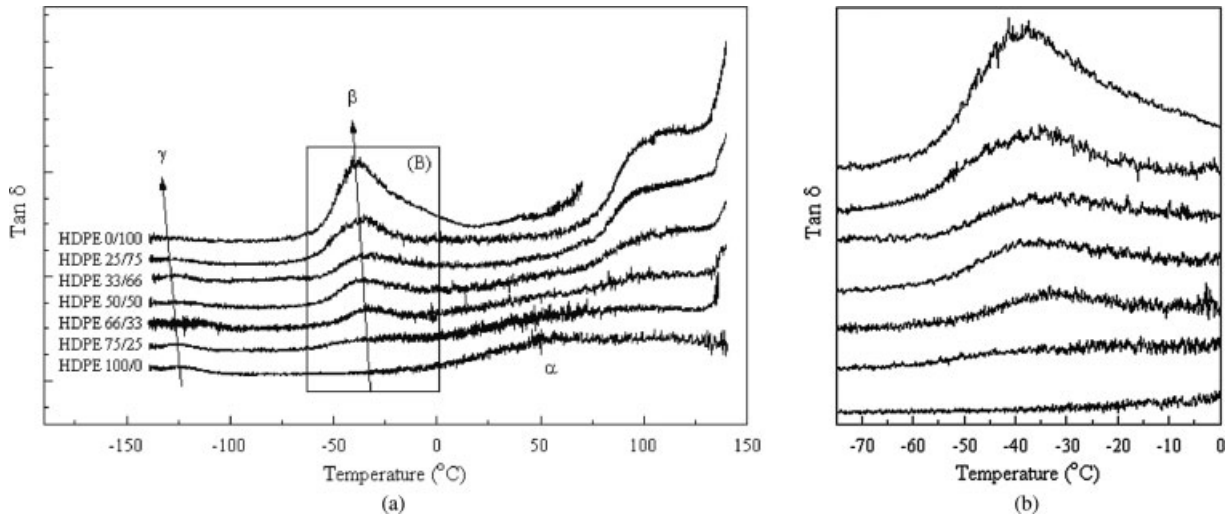


**Figure 5** The tan $\delta$ vs. temperature profile for HDPE/RET blends: (A) over the entire heat profile; (B) over the $\beta$ transition.

behavior of HDPE 100/0 is characteristic of the necking behavior displayed in semicrystalline polymers due to a spherulitic morphology.[30] However, when RET is added to semicrystalline HDPE, a number of mechanisms of plastic deformation contribute to the overall failure. The addition of RET to HDPE greatly increases the extension-to-failure but decreases strength. Visual observations of the tensile fracture surfaces of HDPE 75/25 and HDPE 66/33 showed excessive formation of deformed fibrils. All other blends showed crazing dominant failure characteristic of lamellar separation, shear, and slip as in high-density polyethylene.[30,31] Fibrillous failure is seen in Figure 6 in the step-wise strength drop and extension-to-failure curves characteristic of these blends (HDPE 75/25; HDPE 66/33). The maximum tensile strength as a function of RET content is shown in Figure 7. The near-linear relationship suggests rule of mixture type behavior as the two constituent polymers (HDPE and RET) are blended with good interfacial adhesion. A large variation from linearity might suggest poor interfacial adhesion between the two phases.[20] Fibril formation in HDPE 75/25 and HDPE 66/33 may suggest the elongation of amorphous tie chains followed by slip and tilting of crystalline lamellar chains and orientation of blocks of crystals along the tensile axis.[31]

### Adhesive strength of metal/polymer/metal lap-shear joints

The adhesive properties of HDPE/RET blends were characterized between steel substrates by lap-shear tensile testing. Typical curves for adhesive lap-shear testing of HDPE, RET, and a HDPE/RET blend are

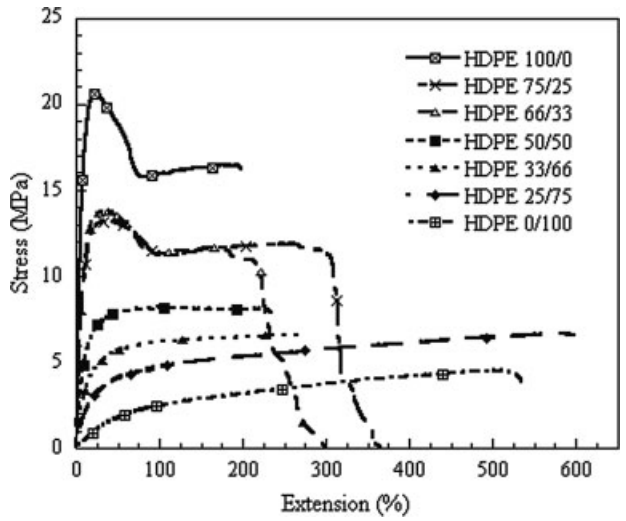


**Figure 6** Typical stress–extension curves for HDPE, RET, and their blends at a displacement rate of 50 mm/min.

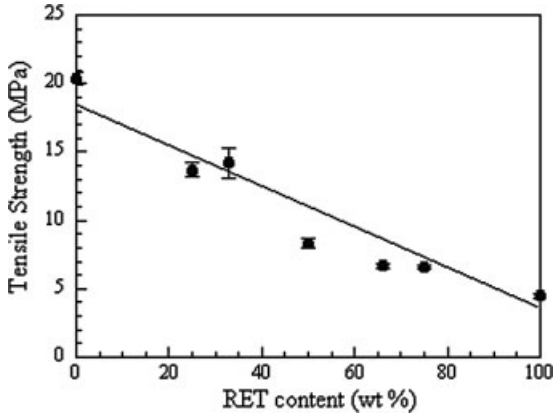


**Figure 7** Tensile strength as a function of RET content for HDPE/RET blends.

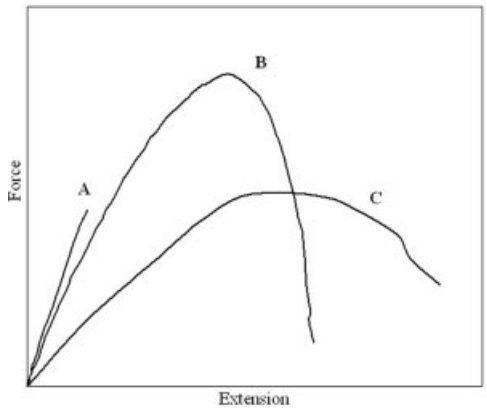


**Figure 8** Typical lap-shear adhesion curves for HDPE/RET blends: (A) HDPE 100/0; (B) HDPE 66/33; and (C) HDPE 0/100.

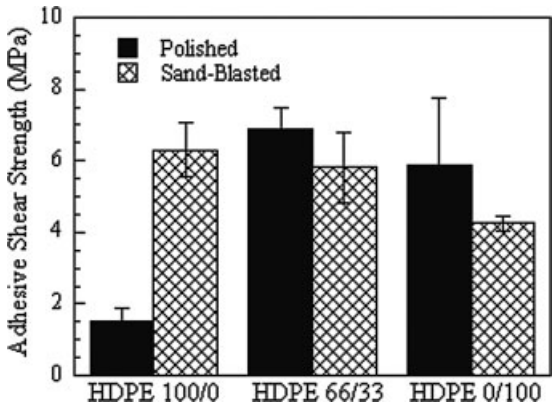


**Figure 10** The effect of surface pretreatments on lap-shear joints using HDPE, RET, and a HDPE/RET blend as the adhesive agent.

represented as curves A, B, and C in Figure 8. Curve A shows the linear behavior of HDPE before catastrophic failure, curve B illustrates linear and continuous yielding with slow softening to failure of the HDPE/RET blend, while curve C shows the significant ductility and extension-to-failure of pure RET. Figure 9 shows the adhesive performance of HDPE hot-melts with the addition of RET. The adhesion measurements of HDPE/RET blends vary slightly with the incorporation of RET. While an increase in adhesive strength with RET content would be expected due to the increase in available polar groups, only a subtle peak in adhesive strength between metallic substrates occurs at 33 wt % RET. This may be understood to be due to competing cohesive/adhesive properties within the polymer blend where HDPE provides tensile strength and RET provides the functional groups necessary for polymer/metal adhesion. Visual observations of the failure surfaces show adhesive failure in HDPE 100/0 where the polymer is completely intact to one metal surface but there is no residual polymer bound to the other metal lap-shear coupon. However, as RET content increases, failure mode shifts to cohesive failure where residual polymer is left on both lap-shear substrate surfaces as failure occurs in the polymer layer.

The lap-shear adhesive strength of HDPE 100/0, HDPE 66/33, and HDPE 0/100 samples was measured with the incorporation of two different surface pretreatments and a silane coupling agent of varying concentration. Changing silane layer thickness will influence bonding characteristics and influence the strength of the polymer/metal bond.[32] Figure 10 shows the change in adhesive performance between polished and sand-blasted steel surfaces. In the case of HDPE 100/0, the adhesive mechanism of mechanical interlock is dominant in grit-blasted steel surfaces as shown by the large increase in adhesive performance. However, in RET and the RET-containing blend, polished surfaces provided increased adhesion most likely due to optimized surface wetting associated with the high surface energy substrate.

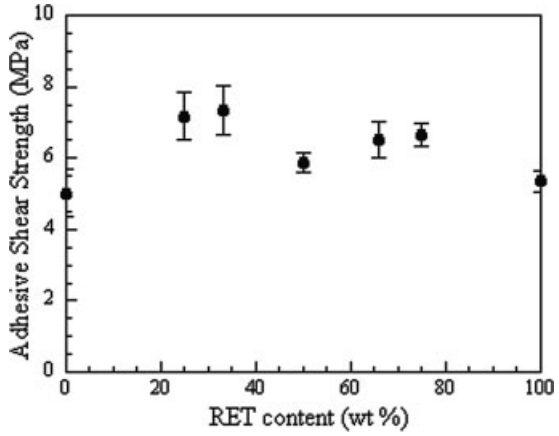


**Figure 9** Adhesive strength as a function of RET content for HDPE/RET blends.

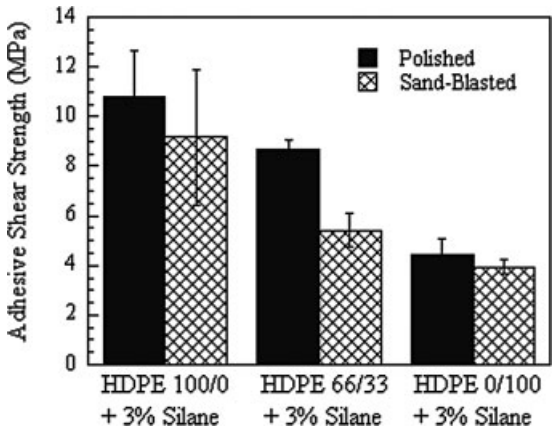


**Figure 11** The effect of a 3% silane coupling agent applied to surface-pretreated steel in lap-shear adhesive testing.

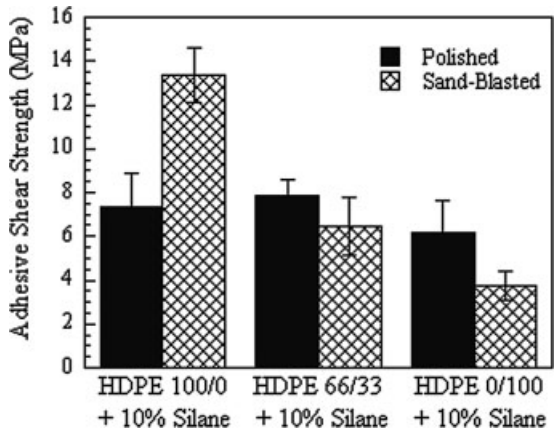


**Figure 12** The effect of a 10% silane coupling agent applied to surface-pretreated steel in lap-shear adhesive testing.

The use of a silane coupling agent to promote adhesion between steel surfaces is shown in Figures 11 and 12. No significant deviation is seen in RET and RET-containing between a 3% and 10% silane agent. However, in the case of HDPE 100/0 with 10% silane treatment, optimized adhesion is seen in the grit-blasted condition. HDPE 66/33 in conjunction with the 3% silane coupling agent on polished steel substrates exhibits the highest adhesive strength of RET-containing blends, ~9 MPa.

## CONCLUSIONS

A reactive ethylene terpolymer, Elvaloy, was compounded at various compositions with HDPE to develop a coating material for steel. On the basis of the DSC and SEM observations, blends of HDPE/RET were found to be immiscible in all compositions. The percent crystallinity and melting temperature of HDPE decrease slightly with increased RET content. The linear relationship of tensile strength with RET additions, suggests good interfacial adhesion which is to be expected in an olefin/olefin-containing blend. Overall, strain to failure is increased with RET content. As RET was added to HDPE resin, adhesive properties increased only slightly in lap-shear joints at 33 wt % RET. Lower RET composition (25–33 wt %) blends show the best overall performance potential for coatings: moderate tensile strength (~13 MPa), a large strain-to-failure (300–400% extension), and increased adhesive properties when bonded to steel (8–10 MPa).

The authors thank the E.I. DuPont de Nemours and Company for financial support of this work and the donation of raw materials. The authors also gratefully acknowledge the assistance of Ms. Evelyn York of the Unified Laboratory Facility at the Scripps Institution of Oceanography at the University of California, San Diego in the operation of the scanning electron microscope.

## References

1. Klechka, E. W. Mater Perform 2000, 39, 46.
2. Xu, C.; Ramani, K.; Kumar, G. Int J Adhes Adhes 2002, 22, 187.
3. Ageorges, C.; Ye, L.; Hou, M. Compos A Appl Sci Manuf 2001, 32, 839.
4. O'Connor, A. E.; Macosko, C. W. J Appl Polym Sci 2002, 86, 3355.
5. Fernandes, E. G.; Lombardi, A.; Solaro, R.; Chiellini, E. J Appl Polym Sci 2001, 80, 2889.
6. Roy, D.; Simon, G. P.; Forsyth, M. Polym Eng Sci 2002, 42, 781.
7. Novák, I.; Krupa, I.; Luyt, A. S. J Appl Polym Sci 2005, 95, 1164.
8. Roy, D.; Simon, G. P.; Forsyth, M. J Polym Mater 2002, 19, 309.
9. Pesetskii, S. S.; Jurkowski, B.; Kuzavkov, A. I. Int J Adhes Adhes 1998, 18, 351.
10. Bright, K.; Malpass, B. W. Eur Polym J 1968, 4, 431.
11. Gauthier, M.; Eisenberg, A. Macromolecules 1989, 22, 3756.
12. Kalfoglou, N. K.; Skafidas, D. S. Eur Polym J 1994, 30, 933.
13. Ajji, A. Polym Eng Sci 1995, 35, 64.
14. Boykin, T. L.; Ciacco, J.; Moore, R. B. Am Chem Soc Polym Prepr Div Polym Chem 1996, 37, 717.
15. Zhao, H.; Tang, T.; Wang, Z.; Huang, B. J Appl Polym Sci 1999, 71, 967.
16. Retolaza, A.; Eguiazábal, J. I.; Nazábal, J. Polym Eng Sci 2002, 42, 2072.
17. Leewajanakul, P.; Pattanaolarn, R.; Ellis, J. W.; Nithitanakul, M.; Grady, B. P. J Appl Polym Sci 2003, 89, 620.
18. Pietrasanta, Y.; Robin, J.; Torres, N.; Boutevin, B. Macromol Chem Phys 1999, 200, 142.
19. Darras, O.; Sequela, R. Polymer 1993, 34, 2946.
20. Cho, K.; Jeon, H. K.; Moon, T. J. J Mater Sci 1993, 28, 6650.
21. Horrion, J.; Agarwal, P. K. Polym Commun 1989, 30, 264.
22. Fairley, G.; Prud'homme, R. E. Polym Eng Sci 1987, 27, 1495.
23. Kyu, T.; Vadhar, P. J Appl Polym Sci 1986, 32, 5575.
24. Kyu, T.; Hu, S. R.; Stein, R. S. J Polym Sci Part B: Polym Phys 1987, 25, 71.
25. Khonakdar, H. A.; Wagenknecht, U.; Jafari, S. H.; Hässler, R.; Eslami, H. Adv Polym Technol 2004, 23, 307.
26. Muñoz, P.; Werlang, M. M.; Yoshida, V. P.; Mauler, R. S. J Appl Polym Sci 2002, 83, 2347.
27. Tsai, C. H.; Chang, F. C. J Appl Polym Sci 1996, 61, 321.
28. Lee, H.; Cho, K.; Ahn, T.; Choe, S.; Kim, I.; Park, I. J Polym Sci Part B: Polym Phys 1997, 35, 1633.
29. Brydson, J. Plastic Materials; Butterworth-Heinemann: London, 1979.
30. Na, B.; Zhang, Q.; Wang, Y.; Fu, Q. Polym Int 2004, 53, 1078.
31. Dasari, A.; Misra, R. D. Mater Sci Eng A 2004, 367, 248.
32. Lenhart, J. L.; Dunkers, J. P.; van Zanten, J. H.; Parnas, R. S. J Colloid Interface Sci 2003, 257, 398.